

Accurate Measurement of Bicycle Parameters

Jason K. Moore*, Mont Hubbard*, A. L. Schwab†, J. D. G. Kooijman†

* Department of Mechanical and Aerospace Engineering
University of California, Davis
One Shields Avenue, Davis, CA, 95616, USA
e-mail: jkmoor@ucdavis.edu, mhubbard@ucdavis.edu

† Laboratory for Engineering Mechanics
Delft University of Technology
Mekelweg 2, 2628CD Delft, The Netherlands
e-mail: a.l.schwab@tudelft.nl, jodikooijman@gmail.com

ABSTRACT

Accurate measurements of a bicycle's physical parameters are required for realistic dynamic simulations and analysis. The most basic models require the geometry, mass, mass location and mass distributions for the rigid bodies. More complex models require estimates of tire characteristics, human characteristics, friction, stiffness, damping, etc. In this paper we present the measurement of the minimal bicycle parameters required for the benchmark Whipple bicycle model presented in [7]. This model is composed of four rigid bodies, has ideal rolling and frictionless joints, and is laterally symmetric. A set of 25 parameters describes the geometry, mass, mass location and mass distribution of each of the rigid bodies. The experimental methods used to estimate the parameters described herein are based primarily on the work done in [3] but have been refined for improved accuracy and methodology. Kooijman's work was preceded by [10] who measured a bicycle in a similar fashion and both [1] and [12] who used similar techniques with scooters.

We measured the physical characteristics of six different bicycles, two of which were set up in two different configurations. The six bicycles, chosen for both variety and convenience, are as follows: *Batavus Browser*, a Dutch style city bicycle measured with and without instrumentation as described in [6]; *Batavus Stratos Deluxe*, a Dutch style sporty city bicycle; *Batavus Crescendo Deluxe* a Dutch style city bicycle with a suspended fork; *Gary Fisher Mountain Bike*, a hardtail mountain bicycle; *Bianchi Pista*, a modern steel frame track racing bicycle; and *Yellow Bicycle*, a stripped down aluminum frame road bicycle measured in two configurations, the second with the fork rotated in the headtube 180 degrees for larger trail.

These eight different parameter sets can be used with, but are not limited to, the benchmark bicycle model. The accuracy of all the measurements are presented up through the eigenvalue prediction of the linear model. The accuracies are based on error propagation theory with correlations taken into account.

Keywords: bicycle, parameters, eigenvalues, Bode.

1 INTRODUCTION

This work is intended to document the indirect measurement of eight real bicycles' physical parameters. The physical parameters measured are those needed for the benchmark Whipple bicycle

model presented in [7]. The work is based on techniques used to measure the instrumented bicycles in [3], [5] and [8]. We improve upon these methods by both increasing and reporting the accuracies of the measurements and by measuring the complete moments of inertia of the frame and fork needed for analysis of the nonlinear model. Furthermore, very little data exists on the physical parameters of different types of bicycles and this work aims to provide a small sample of bicycles.

Döhring [1] and Singh and Goel [12] measured the physical parameters of scooters. Roland and Massing [10] measured the physical parameters of a bicycle in much the same way as is presented, including calculations of uncertainty from the indirect measurement techniques. Patterson [9] used a swing to measure the inertia of a bicycle and rider. The present work is based on the work done by Kooijman [3] using much of the same apparatus and refining the measurement technique.

2 BENCHMARK BICYCLE MODEL

Recently, the Whipple bicycle model has been benchmarked [7] and this model is widely used for bicycle dynamics studies. The unforced two degree-of-freedom, $\mathbf{q} = [\text{steer and roll}]$, model takes the form:

$$\mathbf{M}\ddot{\mathbf{q}} + v\mathbf{C}_1\dot{\mathbf{q}} + [g\mathbf{K}_0 + v^2\mathbf{K}_2]\mathbf{q} = 0 \quad (1)$$

where the entries of the \mathbf{M} , \mathbf{C}_1 , \mathbf{K}_0 and \mathbf{K}_2 matrices are combinations of 25 bicycle physical parameters that include the geometry, mass, mass location and mass distribution of the four rigid bodies. The 25 parameters presented in [7] are not necessarily a minimum set for the Whipple model, as shown in [11], but are useful as they represent more intuitively measurable quantities. Furthermore, many more parameters are not needed due to the assumptions of the Whipple model such as no-slip tires, lateral symmetry, knife edge wheels, etc.

3 BICYCLE DESCRIPTIONS

We choose to measure the physical parameters of six bicycles Fig. 1. The three Batavus bicycles were donated by the manufacturer. We asked for a bicycle that they considered stable and one that they did not. They claimed the Browser was a “stable” bicycle and that the Stratos was “nervous”. The Fisher and the Pista were chosen to provide some variety, a mountain and road bike. The yellow bike is used to demonstrate bicycle stability.

Batavus Browser (B, B*) The Batavus Browser Fig. 1a is an average priced Dutch city bike. It has a steel frame, a three speed internal rear hub, handle bars for an upright posture and includes various accessories for utility purposes. We measured the physical properties of the stock Browser model and also equipped with the instrumentation used in our other experiments [4].

Batavus Crescendo Deluxe (C) The Batavus Crescendo Deluxe Fig. 1b is also a Dutch city bike for touring. It has an aluminum frame, an eight speed internal hub, upright handlebars, accessories for utility and a suspension fork and suspension seatpost.

Gary Fisher Ziggurat (G) The Gary Fisher Ziggurat Fig. 1c is a modern lightweight front suspended mountain bike. It has a aluminum frame, large low pressure mountain bike tires, and is for racing with few extra accessories.

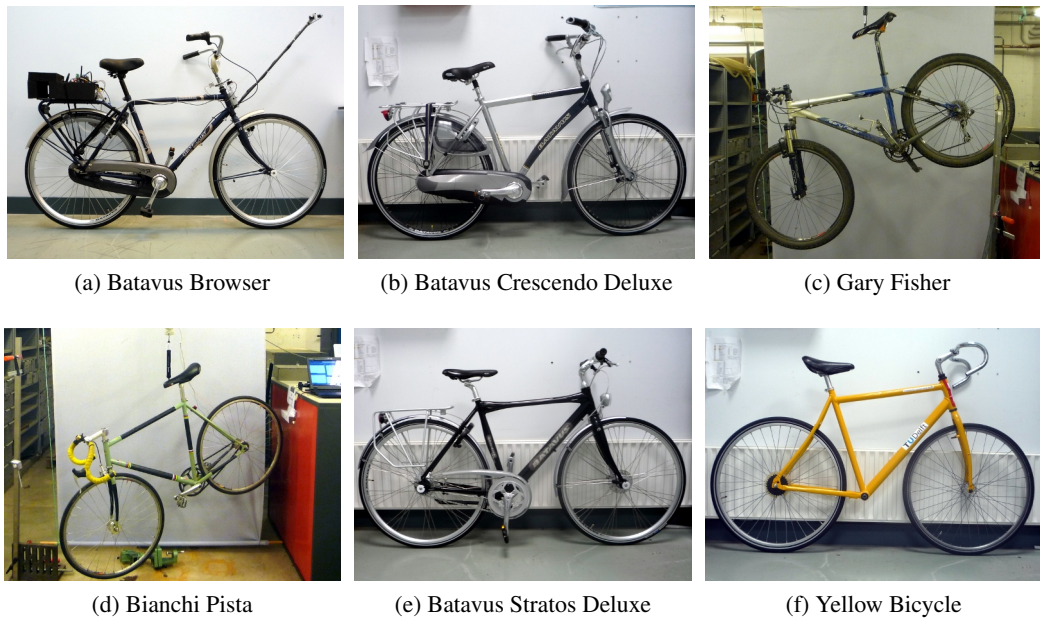


Figure 1: The six bicycles measured in the experiments. The Batavus Browser (a) is shown with the instrumentation and the Yellow Bicycle (f) is shown with its fork reversed.

Bianchi Pista (P) The Bianchi Pista Fig. 1d is a modern lightweight steel track bicycle. It has a single gear ratio and minimal extras to keep the weight low. It has drop handlebars and high pressure racing tires.

Batavus Stratos Deluxe (S) The Batavus Stratos Deluxe Fig. 1e is a sporty Dutch city bicycle. The frame is aluminum. It has a seven-speed internal hub and mountain style handle bars for a less upright seating posture, but also includes accessories for utility such as a rear rack, fenders, light and chainguard.

Yellow Bicycle (Y, Y*) The yellow bicycle Fig. 1f is used in the lab to demonstrate that a bicycle is stable at certain speeds. It is an aluminum road frame of unknown make with the most of components removed. The wheels, drop handlebar, seat, seat post and bottom bracket are the only parts on the bike. This bicycle was measured with both the fork in normal position and reversed. The fork was reversed to "decrease the minimal stable speed" [3] of the bicycle.

4 PARAMETERS

The 25 parameters can be estimated using many techniques. Where possible we measured the benchmark parameter directly.

5 ACCURACY

We took great care to improve and report the accuracy of the measurements of the parameters. Following the thrust of [10] we used error propagation theory to calculate accuracy of the 25 benchmark parameters. We start by estimating the standard deviation of the actual measurements

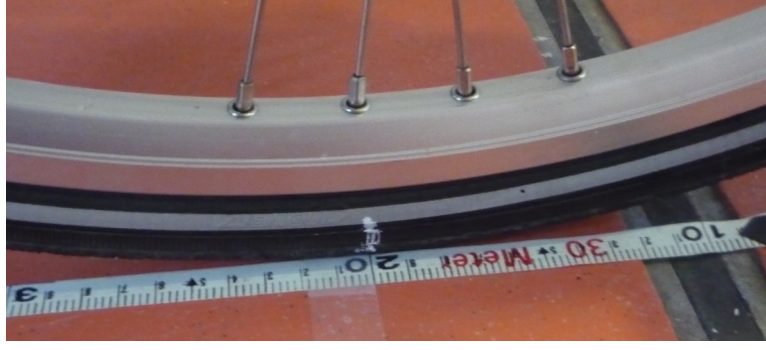


Figure 2: Wheel and tire with chalk mark aligned to the tape measure.

taken. If x is a parameter and is a function of the measurements, u, v, \dots , then x is a random variable defined as $x = f(u, v, \dots)$. The sample variance of x is defined as

$$s_x^2 = \frac{1}{N-1} \sum_{i=1}^N \left[(u_i - \bar{u})^2 \left(\frac{\partial x}{\partial u} \right)^2 + (v_i - \bar{v})^2 \left(\frac{\partial x}{\partial v} \right)^2 + 2(u_i - \bar{u})(v_i - \bar{v}) \left(\frac{\partial x}{\partial u} \right) \left(\frac{\partial x}{\partial v} \right) + \dots \right] \quad (2)$$

Using the definitions for variance and covariance, Equation 2 can be simplified to

$$s_x^2 = s_u^2 \left(\frac{\partial x}{\partial u} \right)^2 + s_v^2 \left(\frac{\partial x}{\partial v} \right)^2 + 2s_{uv} \left(\frac{\partial x}{\partial u} \right) \left(\frac{\partial x}{\partial v} \right) + \dots \quad (3)$$

If u and v are uncorrelated then $s_{uv} = 0$. Most of the calculations hereafter have uncorrelated variables but a few do not and the covariance has to be taken into account. Equation 3 can be used to calculate the variance of all types of functions. Simple addition of two random variables may be the most basic example:

$$x = au + bv \quad (4)$$

$$s_x = a^2 s_u^2 + b^2 s_v^2 \quad (5)$$

6 GEOMETRY

6.1 WHEEL RADII

The radii of the front r_F and rear r_R wheels were estimated by measuring the linear distance traversed along the ground through either 13 or 14 rotations of the wheel. Each wheel was measured separately and the measurements were taken with a 72kg rider seated on the bicycle. A 30 meter tape measure (resolution: 2mm) was pulled tight and taped on a flat level smooth floor. The tire was marked with chalk and aligned with the tape measure Fig. 2. The accuracy of the distance measurement is approximately $\pm 0.01\text{m}$. The tires were pumped to the recommended inflation pressure before the measurements. The wheel radius is calculated by

$$r \pm \sigma_r = \frac{d}{2\pi n} \pm \left(\frac{\sigma_d}{2\pi n} \right) \quad (6)$$

6.2 HEAD TUBE ANGLE

The head tube angle was measured directly using an electronic level with a $\pm 0.2^\circ$ accuracy. The bicycle frame was fixed perpendicular to the ground, the steering angle was set to the nominal, tire pressures were at recommended levels and the bicycle was unloaded. The steer axis tilt λ is the complement to the head tube angle.

$$\lambda \pm \sigma_\lambda = \frac{\pi}{180^\circ} (90^\circ - \lambda_{ht}) \pm \left(\frac{\pi}{180^\circ} \right) \sigma_{\lambda_{ht}} \quad (7)$$

6.3 TRAIL

Trail is difficult to measure directly so we instead chose to measure the fork offset. The fork offset was measured by clamping the steer tube of the front fork into a v-block on a flat table. A ruler was used to measure the height of the center of the head tube and the height of the center of the axle axis. The fork blades were aligned such that the axle axis was parallel to the table surface.

$$c = \frac{r_F \sin \lambda - f_o}{\cos \lambda} \quad (8)$$

$$\sigma_c^2 = \sigma_{r_F}^2 \tan^2 \lambda - \sigma_{f_o}^2 \sec^2 \lambda + \sigma_\lambda^2 (r_F \sec^2 \lambda - f_o \sec \lambda \tan \lambda)^2 \quad (9)$$

6.4 WHEELBASE

We measured the wheelbase with the bicycle in nominal configuration described in Sec. 6.2. We used a tape measure to measure the distance from one wheel axle center to the other with a 0.002 m accuracy.

7 MASS

The total mass of each bicycle was measured using a spring scale with a resolution of 100 grams. The total mass was only used for comparison purposes. Each of the four bicycle parts were measured using a Molen 20 kilogram scale with a resolution of 20 grams. The accuracy was conservatively assumed to also be ± 20 grams.

8 CENTER OF MASS

8.1 WHEELS

The centers of mass of the wheels are assumed to be at their geometrical centers to comply with the Whipple model.

8.2 REAR FRAME

The rear frame was hung in three orientations as a torsional pendulum (both for the center of mass measurements and the moment of inertia measurements described in Sec. 9). We assumed that the frame was laterally symmetric, complying with the Whipple model. The frame could rotate about a joint such that gravity aligned the center of mass with the pendulum axis. The orientation angle of the headtube, α_B , Fig. 4a relative to the earth was measured using a digital level ($\pm 0.2^\circ$ accuracy), Figure 5a. A string was aligned with the pendulum axis and allowed to pass by the



Figure 3: The scale used to measure the mass of each bicycle component.

frame. The horizontal distance a_B between the rear axle and the string was measured by aligning a ruler perpendicular to the string. The distance a_B was negative if the string fell to the right of the rear axle and positive if it fell to the left of the rear axle. These measurements allow for the calculation of the center of mass location in the global reference frame. The frame rotation angle β_B is defined as rotation of the frame in the nominal configuration to the hanging orientation, rotated about the Y axis.

$$\beta = \lambda - \alpha \quad (10)$$

$$\sigma_\beta^2 = \sigma_\lambda^2 + \sigma_\alpha^2 \quad (11)$$

The center of mass can be found by realizing that the pendulum axis X_P is simply a line in the nominal bicycle reference frame with a slope m and a z -intercept b where the i subscript corresponds the different frame orientations Fig. 4b. The slope can be shown to be

$$m_i = -\tan \beta_i \quad (12)$$

$$\sigma_m^2 = \sigma_\beta^2 \sec^4 \beta \quad (13)$$

The z -intercept can be shown to be

$$b_i = -\left(\frac{a_B}{\cos \beta_i} + r_R\right) \quad (14)$$

$$\sigma_b^2 = \sigma_a^2 \sec^2 \beta + \sigma_{r_R}^2 + \sigma_\beta^2 a^2 \sec^2 \beta \tan^2 \beta \quad (15)$$

Theoretically, the center of mass lies on each line but due to experimental error, if there are more than two lines, the lines do not cross all at the same point. Only two lines are required to calculate the center of mass of the laterally symmetric frame, but more orientations increase the center of mass measurement accuracy. The three lines are defined as:

$$z = m_i x + b_i \quad (16)$$

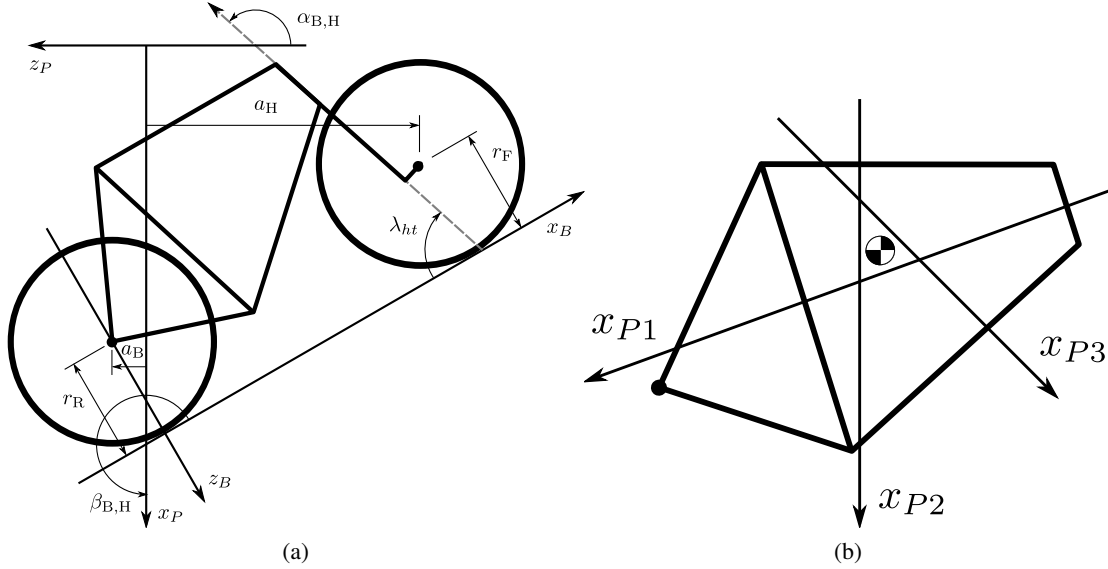


Figure 4: (a) Pictorial description of the angles and dimensions that related the nominal bicycle reference frame XYZ_B with the pendulum reference frame XYZ_P . (b) Exaggerated intersection of the three pendulum axes and the location of the center of mass.

The mass center location can be calculated by finding the intersection of these three lines. Two approaches were used to calculate the center of mass. Intuition lead us to think that the center of mass is located at the centroid of the triangle made by the three intersecting lines. The centroid can be found by calculating the intersection point of each pair of lines and then averaging the three intersection points.

$$\begin{bmatrix} -m_1 & 1 \\ -m_2 & 1 \end{bmatrix} \begin{bmatrix} x_a \\ z_a \end{bmatrix} = \begin{bmatrix} b_1 \\ b_2 \end{bmatrix} \quad (17)$$

$$x_B = \frac{x_a + x_b + x_c}{3} \quad (18)$$

$$z_B = \frac{z_a + z_b + z_c}{3} \quad (19)$$

Alternatively, the three lines can be treated as an over determined linear system and the least squares method is used to find a unique solution. This solution is not the same as the triangle centroid method.

$$\begin{bmatrix} -m_1 & 1 \\ -m_2 & 1 \\ -m_3 & 1 \end{bmatrix} \begin{bmatrix} x_B \\ z_B \end{bmatrix} = \begin{bmatrix} b_1 \\ b_2 \\ b_3 \end{bmatrix} \quad (20)$$

The solution with the higher accuracy is the preferred one.

8.3 Fork

The fork and handlebars are a bit trickier to hang in three different orientations. Typically two angles can be obtained by clamping to the steer tube at the top and the bottom. The third angle can be obtained by clamping to the stem. The center of mass of the fork is calculated in the same fashion. The slope of the line in the benchmark reference frame is the same as for the frame but the z-intercept is different:

$$b = w \tan \beta - r_F - \frac{a}{\cos \beta} \quad (21)$$

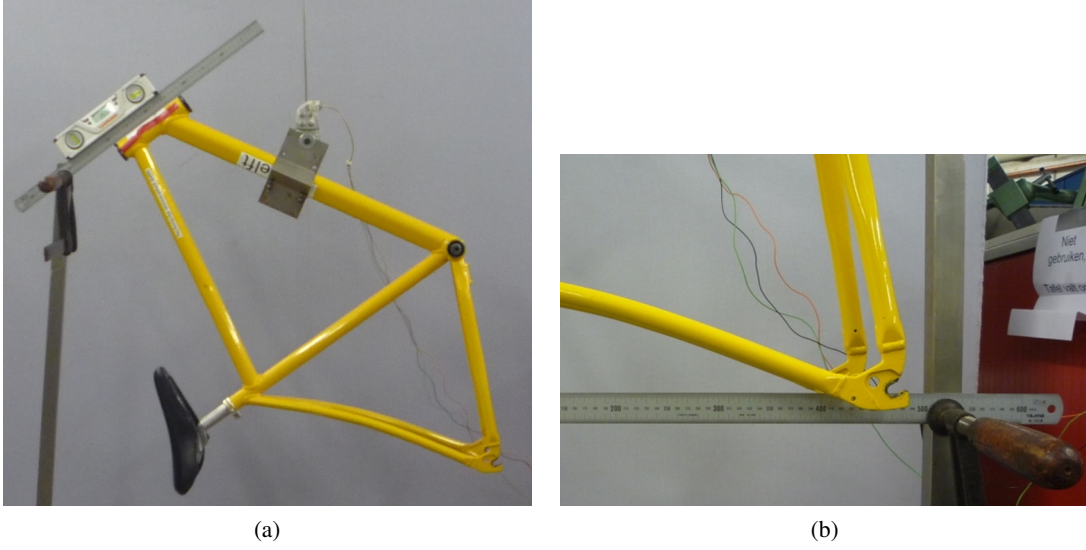


Figure 5: (a) The digital level was mounted to a straight edge aligned with the headtube of the bicycle frame. This was done without allowing the straight edge to touch the frame. The frame wasn't completely stationary so this was difficult. The light frame oscillations could be damped out by submerging a low hanging area of the frame into a bucket of water to decrease the oscillation. (b) Measuring the distance from the pendulum axis to the rear wheel axle using level ruler.

$$\sigma_b^2 = \sigma_w^2 \tan^2 \beta + \sigma_\beta^2 (w \sec^2 \beta - a \sec \beta \tan \beta)^2 + \sigma_{r_F}^2 + \sigma_a^2 \sec^2 \beta \quad (22)$$

9 MOMENT OF INERTIA

The moments of inertia of the wheels, frame and fork were measured by taking advantage of the assumed symmetry of the parts and by hanging the parts as both compound and torsional pendulums and measuring their periods of oscillation when perturbed at small angles. The rate of oscillation was measured using a [Silicon Sensing CRS03 100 deg/s rate gyro](#). The rate gyro was sampled at 1000hz with a [National Instruments USB-6008 12 bit data acquisition unit](#) and MATLAB. The measurement durations were either 15 or 30 secs and each moment of inertia measurement was performed three times. No extra care was taken to calibrate the rate gyro, maintain a constant power source (i.e. the battery drains slowly), or account for drift. The raw voltage signal was used to determine only the period of oscillation which is needed for the moment of inertia calculations. The function Eqn 23 was fit to the data using a nonlinear least squares fit routine for each experiment to determine the quantities A , B , C , ζ , and ω .

$$f(t) = A + e^{-\zeta\omega t} \left[B \sin \sqrt{1 - \zeta^2}\omega t + C \cos \sqrt{1 - \zeta^2}\omega t \right] \quad (23)$$

Most of the data fit the damped oscillation function well with very light (and ignorable) damping. There were several instances of beating-like phenomena for some of the parts at particular orientations. Roland and Massing [10] also encountered this problem and used a bearing to prevent the torsional pendulum from swinging. Figure 7 shows an example of the beating like phenomena.

The physical phenomenon observed corresponding to data sets such as these was that the bicycle frame or fork was perturbed torsionally. After set into motion the torsional motion died out and a longitudinal swinging motion increased. The motions alternated back and forth with neither ever reaching zero. The frequencies of these motions were very close to one another and it is not

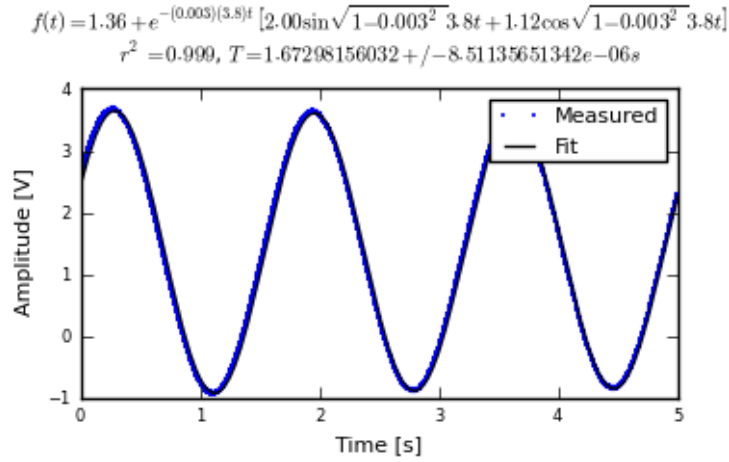


Figure 6: Example of the raw voltage data taken during a 30 second measurement of the oscillation of one of the components.

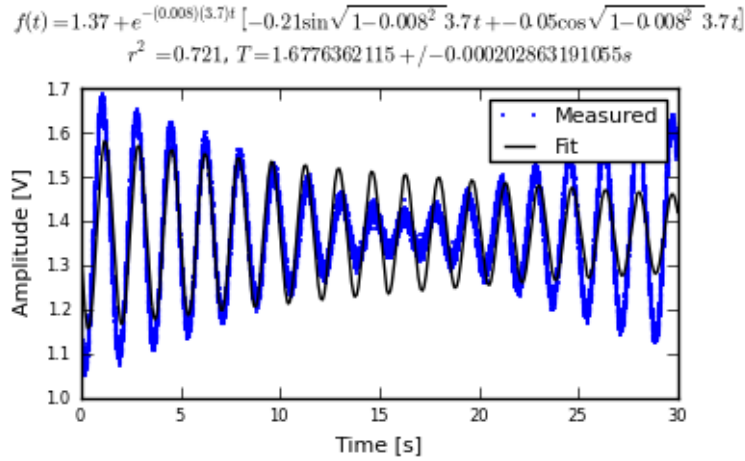


Figure 7: An example of the beating-like phenomena observed on 5% of the experiments.

apparent how dissect the two. We explored fitting to a function such as

$$f(t) = A \sin(\omega_1 t) + B \sin(\omega_2 t + \phi) + C \quad (24)$$

But the fit predicts that ω_1 and ω_2 are very similar frequencies. There was no easy way to choose which of the two ω 's was the one associated with the torsional oscillation. Some work was done to model the torsional pendulum as a laterally flexible beam to determine this, but we thought accuracy of the period calculation would not improve enough for the effort required. Future experiments should simply prevent the swinging motion of the pendulum without damping the torsional motion.

The period for a damped oscillation is

$$T = \frac{2\pi}{\sqrt{1 - \zeta^2 \omega_n}} \quad (25)$$



Figure 8: The rigid pendulum fixture mounted to a concrete column.

The uncertainty in the period, T , can be determined from the fit. Firstly, the variance of the fit is

$$\sigma_y^2 = \frac{1}{N-5} \sum_{i=1}^N (y_{mi} - \bar{y}_m)^2 - (y_{pi} - \bar{y}_m)^2 \quad (26)$$

The covariance matrix of the fit function can be formed

$$\mathbf{U} = \sigma_y^2 \mathbf{H}^{-1} \quad (27)$$

where \mathbf{H} is the Hessian [2]. \mathbf{U} is a 5×5 matrix with the variances of each of the five fit parameters along the diagonal. The variance of T can be computed using the variance of ζ and ω . It is important to note that the uncertainties in the period are very low ($< 1e-4$), even for the fits with low r^2 values.

9.1 TORSIONAL PENDULUM

A torsional pendulum was used to measure all moments of inertia about axes in the laterally symmetric plane of each of the wheels, fork and frame. The pendulum is made up of a rigid mount, an upper clamp, a torsion rod, and various lower clamps. A 5 mm diameter, 1 m long mild steel rod was used as the torsion spring. A lightweight, low relative moment of inertia clamp was constructed that could clamp the rim and the tire. The moments of inertia of the clamps were neglected. The wheel was hung freely such that the center of mass aligned with the torsional pendulum axis and then secured. The wheel was then perturbed and oscillated about the pendulum axis. The rate gyro was mounted on the clamp oriented along the pendulum axis.

The torsional pendulum was calibrated using a known moment of inertia Fig. 9. A torsional pendulum almost identical to the one used in [3] was used to measure the average period \bar{T}_i of oscillation of the rear frame at three different orientation angles β_i , where $i = 1, 2, 3$, as shown in Fig. 4b. The parts were perturbed lightly, less than 1 degree, and allowed to oscillate about the pendulum axis through at least ten periods. This was done at least three times for each frame and the recorded periods were averaged.

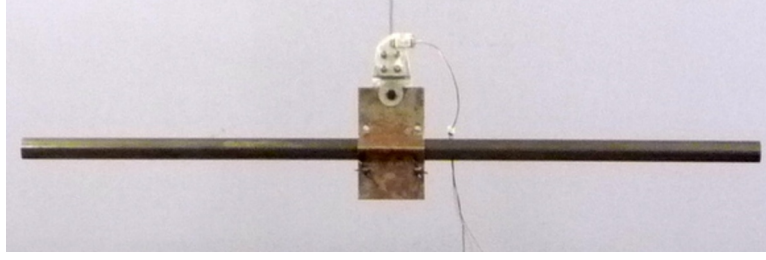


Figure 9: The steel calibration rod. The moment of inertia of the rod, $I = \frac{m}{12}(3r^2 + l^2)$, can be used to estimate the stiffness of the pendulum, $k = \frac{4I\pi^2}{T^2}$, with $k = 5.62 \pm 0.02 \frac{\text{Nm}}{\text{rad}}$

9.2 WHEELS

Finding the full inertia tensors of the wheels is less complex because the wheels are assumed symmetric about three orthogonal planes so products of inertia are zero. The $I_{xx} = I_{zz}$ moments of inertia were calculated by measuring the averaged period of oscillation about an axis in the XZ -plane using the torsional pendulum setup and Eq. 30. The wheels are assumed to be laterally symmetric and about any radial axis. Thus only two moments of inertia are required for the set of benchmark parameters. The moment of inertia about the axle was measured by hanging the wheel as a compound pendulum, Fig. 10b. The wheel was hung on a horizontal rod and perturbed to oscillate about the axis of the rod. This rate gyro was attached to the spokes near the hub and oriented mostly along the axle axis. The wheels tended to precess at the contact point about the vertical axis which added a very low frequency component of rate along the vertical radial axis, but this should not affect the period estimation about the compound pendulum axis. A fixture that prevented precession would be preferable for future measurements. The pendulum arm length is the distance from the rod/rim contact point to the mass center of the wheel. The inner diameter of the rim was measured and divided by two to get $l_{F,R}$. The moment of inertia about the axle is calculated from:

$$I_{Ryy} = \left(\frac{\bar{T}}{2\pi}\right)^2 m_R g l_R - m_R l^2 \quad (28)$$

The radial moment of inertia was measured by hanging the wheel as a torsional pendulum, Fig. 10a. The wheel was hung freely such that the center of mass aligned with the torsional pendulum axis and then secured. The wheel was then perturbed and oscillated about the vertical pendulum axis. The radial moment of inertia can be calculated as such:

$$I_{xx} = \frac{k\bar{T}^2}{4\pi^2} \quad (29)$$

9.3 FRAME

Three measurements were made to estimate the globally referenced moments and products of inertia (I_{xx} , I_{xz} and I_{zz}) of the rear frame. The frame was typically hung from the three main tubes: seat tube, down tube and top tube, Fig. 5a. The rear fender prevented easy connection to the seat tube on some of the bikes and the clamp was attached to the fender. The fender was generally less rigid than the frame tube. For best accuracy with only three orientation angles, the frame should be hung at three angles that are 120° apart. The three tubes on the frame generally provide that the orientation angles were spread evenly at about 120° . Furthermore, taking data at more orientation angles could improve the accuracy and is generally possible with standard diamond frame bicycles.

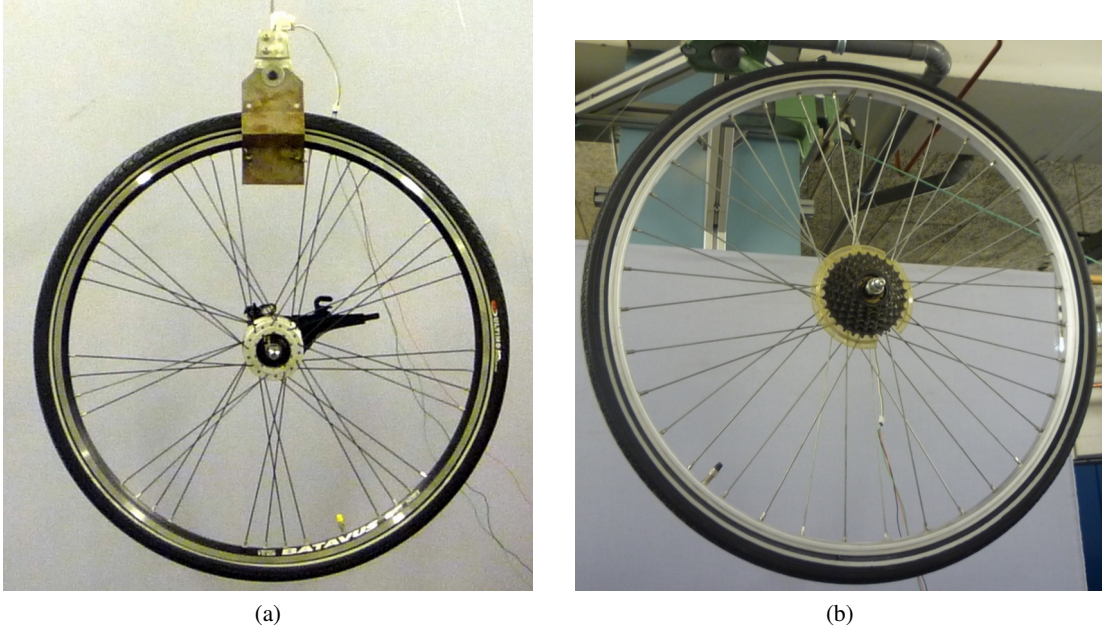


Figure 10: (a) The front wheel of the Crescendo hung as a torsional pendulum. (b) A wheel hung as a compound pendulum.

Three moments of inertia J_i about the pendulum axes were calculated using Eq. 30.

$$J_i = \frac{k\overline{T}_i^2}{4\pi^2} \quad (30)$$

The moments and products of inertia of the rear frame and handlebar/fork assembly with reference to the benchmark coordinate system were calculated by formulating the relationship between inertial frames

$$\mathbf{J}_i = \mathbf{R}_i \mathbf{I} \mathbf{R}_i^T \quad (31)$$

where \mathbf{J}_i is the inertia tensor about the pendulum axes, \mathbf{I} is the inertia tensor in the global reference frame and \mathbf{R} is the rotation matrix relating the two frames, Fig. 4a. The global inertia tensor is defined as

$$\mathbf{I} = \begin{bmatrix} I_{xx} & I_{xz} \\ I_{xz} & I_{zz} \end{bmatrix}. \quad (32)$$

The inertia tensor can be reduced to a 2×2 matrix because the frame is assumed to be laterally symmetric and the y axis of the pendulum reference is the same as the y axis of the benchmark reference frame. The simple rotation matrix about the Y -axis can similarly be reduced to a 2×2 matrix where s_{β_i} and c_{β_i} are defined as $\sin \beta_i$ and $\cos \beta_i$, respectively.

$$\mathbf{R} = \begin{bmatrix} c_{\beta_i} & -s_{\beta_i} \\ s_{\beta_i} & c_{\beta_i} \end{bmatrix} \quad (33)$$

The first entry of \mathbf{J}_i in Eq. 31 is the moment of inertia about the pendulum axis and is written explicitly as

$$J_i = c_{\beta_i}^2 I_{xx} - 2s_{\beta_i} c_{\beta_i} I_{xz} + s_{\beta_i}^2 I_{zz}. \quad (34)$$

Similarly, calculating all three J_i allows one to form

$$\begin{bmatrix} J_1 \\ J_2 \\ J_3 \end{bmatrix} = \begin{bmatrix} c_{\beta_1}^2 & -2s_{\beta_1}c_{\beta_1} & s_{\beta_1}^2 \\ c_{\beta_2}^2 & -2s_{\beta_2}c_{\beta_2} & s_{\beta_2}^2 \\ c_{\beta_3}^2 & -2s_{\beta_3}c_{\beta_3} & s_{\beta_3}^2 \end{bmatrix} \begin{bmatrix} I_{xx} \\ I_{xz} \\ I_{zz} \end{bmatrix} \quad (35)$$



Figure 11: (a) Rear frame hung as a compound pendulum. (b) Browser fork hung as a compound pendulum.

and the moments of inertia can be solved for. The inertia of the frame about an axis normal to the plane of symmetry was estimated by hanging the frame as a compound pendulum at the wheel axis, Fig. 11a. Equation 28 is used but with the mass of the frame and the frame pendulum length.

$$l_B = \sqrt{x_B^2 + (z_B + r_R)^2} \quad (36)$$

9.4 FORK AND HANDLEBAR

The inertia of the fork and handlebar is calculated in the same way as the frame. The fork is hung as both a torsional pendulum, Fig. 12, and as a compound pendulum, Fig. 11b. The fork provides fewer mounting options to obtain at least three equally spaced orientation angles, especially if there is no fender. The torsional calculations follow equations 30 through 35 and the compound pendulum calculations is calculated with equation 28. The fork pendulum length is calculated using

$$l_H = \sqrt{(x_H - w)^2 + (z_B + r_F)^2} \quad (37)$$

10 LINEAR ANALYSIS

Once all bicycle parameters have been calculated the canonical matrices can be formed and the linear dynamics of the bicycles can be explored. The values of the canonical matrices can be found in the second table in Appendix A. We also added the same rigid rider to each bicycle for further

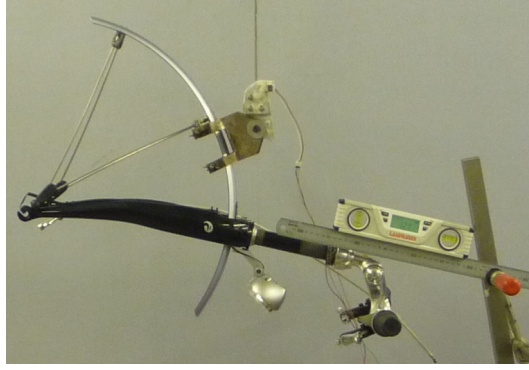


Figure 12: The Stratos fork and handlebar assembly hung as a torsional pendulum.

Table 1: Mass, center of mass and moment of inertia for the rider relative to the benchmark coordinate system from [8]

Parameter	Value
m_P [kg]	72
x_P [m]	0.2909
z_P [m]	-1.1091
I_P [kg m ²]	$\begin{bmatrix} 7.9985 & 0 & -1.9272 \\ 0 & 8.0689 & 0 \\ -1.9272 & 0 & 2.3624 \end{bmatrix}$

comparison. The rigid rider was assumed to be in the same position and posture for each bicycle relative to the rear wheel contact point.

10.1 EIGENVALUES

The eigenvalues of the bicycles with (Fig. 13) and without (Fig. 16) the rider can be plotted versus forward speed. Figure 13 shows that the bikes have the typical characteristics of the benchmark bicycle: four real roots at very slow speeds, two of which are unstable; a complex pair that is unstable at lower speeds and stable at intermediate speeds; and a root that is mildly unstable at higher speeds. The one noticeable difference is that the capsize and caster modes are contained in a complex pair between about 0.5 and 3 m/s. The frequency of oscillation is of comparable magnitude to that of the weave mode. But, the root locus in the real and imaginary plane, Fig. 14, shows that the mode damps out quickly. Examining the eigenvectors reveals that the mode is steer leading roll with a 90 degree phase, both of their magnitudes being similar, Fig 15. With the rider added, the second complex pair disappears and the bikes have the typical characteristics of the benchmark bicycle model. Reversing the fork on the yellow bike lowers the weave critical speed and increases the stable speed range. Also, the addition of weight to the rear rack of the Browser does little to the eigenvalues.

10.2 FREQUENCY RESPONSE

The frequency response of the bicycles (Fig. 17) and bicycle with rider (Fig. 18) also reveal some interesting things. In the steer-torque-to-roll Bode diagram the magnitude difference among bicycles can vary up to 10 dB (or about 8.5 degrees per Newton-meter of torque) for the particular speed shown. The difference in the frequency response for the bicycle with the rigid rider shows

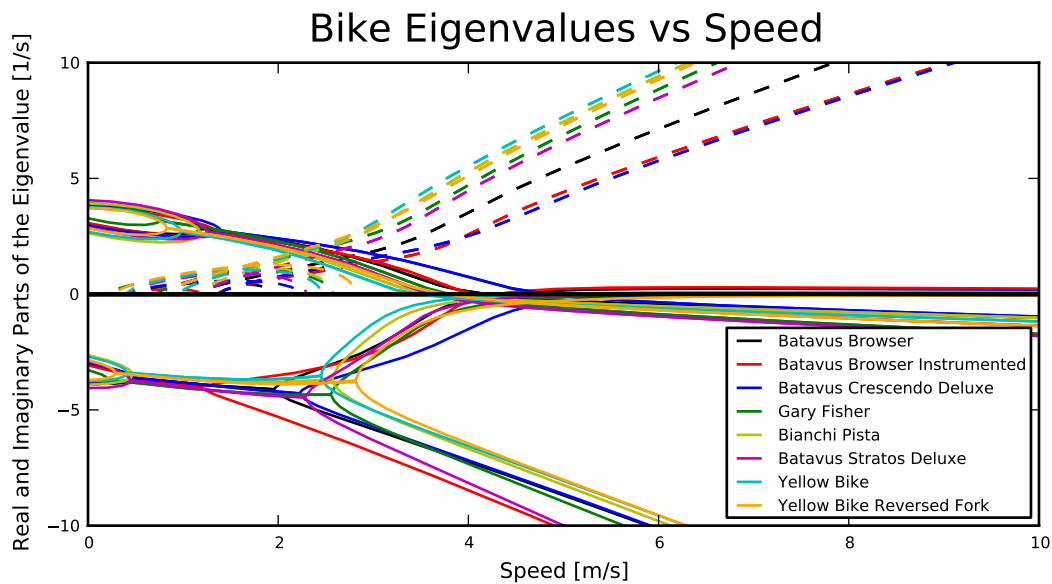


Figure 13: Eigenvalues versus speed for all eight bicycles without the rider.

less variation among the bicycles, Fig. 18, as the rider's mass and inertia play a larger roll.

11 CONCLUSION

We have presented a detailed method to accurately estimate the physical parameters of a bicycle needed for the benchmarked Whipple bicycle model [7]. We measured eight different bicycles providing both the parameter sets and linear model coefficient matrices for the bicycles alone and the bicycles with the same rigid rider. The uncertainties in the parameters and matrix coefficients are included for the bicycle alone. Finally, we have presented a brief comparison of the eight bicycles using eigenanalysis and Bode frequency response.

12 ACKNOWLEDGEMENTS

This material is based upon work partially supported by the National Science Foundation under Grant No. 0928339.

REFERENCES

- [1] DÖHRING, E. *Über die Stabilität und die Lenkkräfte von Einspurfahrzeugen*. PhD thesis, Technical University Braunschweig, Germany, 1953.
- [2] HUBBARD, M., AND ALAWAYS, L. W. Rapid and accurate estimation of release conditions in the javelin throw. *Journal of Biomechanics* 22 (1989), 583–595.
- [3] KOOIJMAN, J. D. G. *Experimental Validation of a Model for the Motion of an Uncontrolled Bicycle*. MSc thesis, Delft University of Technology, 2006.

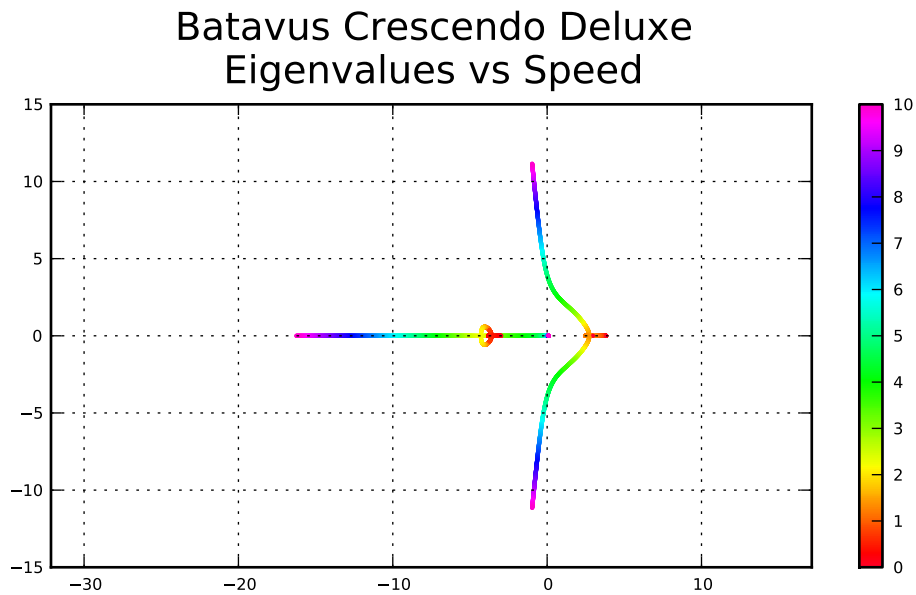


Figure 14: The root loci with speed as the parameter for the Crescendo.

- [4] KOOIJMAN, J. D. G., AND SCHWAB, A. L. Experimental validation of the lateral dynamics of a bicycle on a treadmill. In *Proceedings of the ASME 2009 International Design Engineering Technical Conferences & Computers and Information in Engineering Conference, IDETC/CIE 2009* (2009), no. DETC2009-86965.
- [5] KOOIJMAN, J. D. G., SCHWAB, A. L., AND MEIJAARD, J. P. Experimental validation of a model of an uncontrolled bicycle. *Multibody System Dynamics 19* (May 2008), 115–132.
- [6] KOOIJMAN, J. D. G., SCHWAB, A. L., AND MOORE, J. K. Some observations on human control of a bicycle. In *Proceedings of the ASME 2009 International Design and Engineering Technical Conferences & Computers and Information in Engineering Conference* (2009).

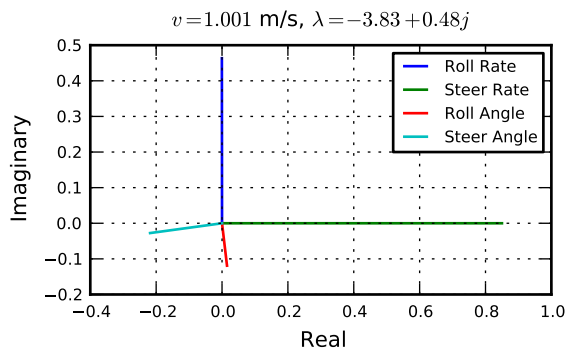


Figure 15: Eigenvector components for the second complex mode pair at low speed.

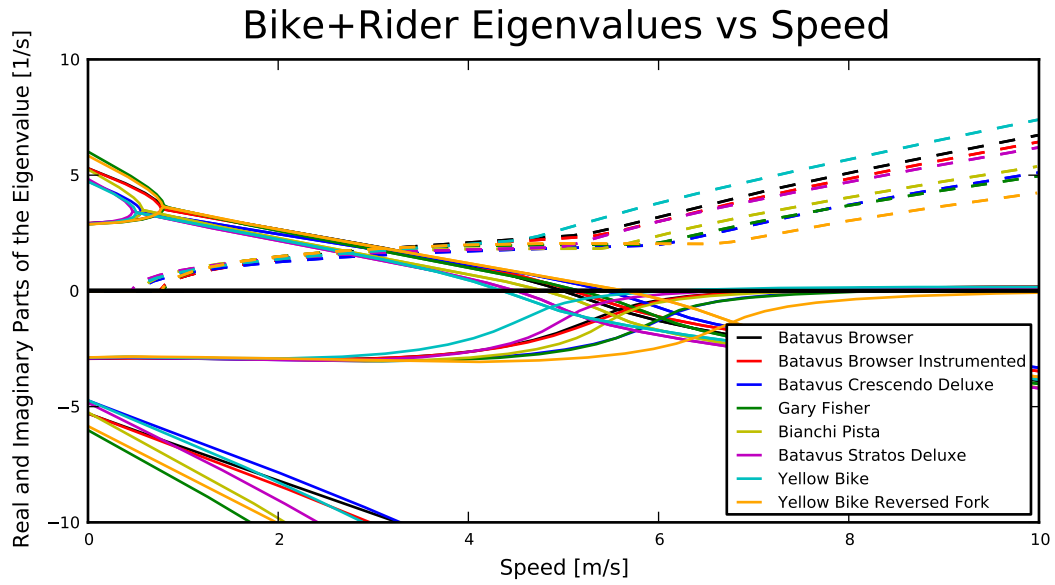


Figure 16: Eigenvalues versus speed for all eight bicycles with the same rigid rider.

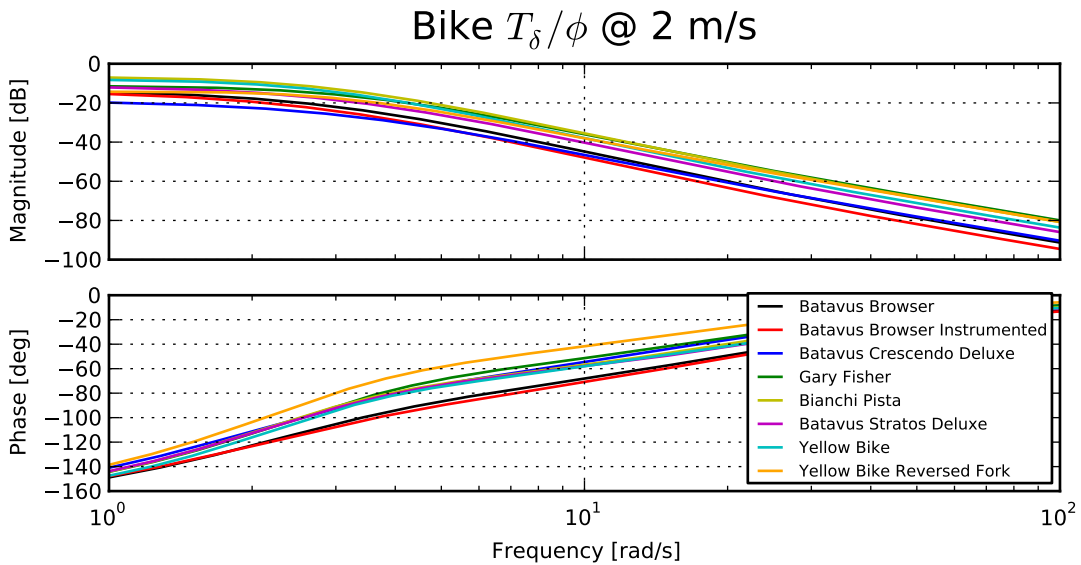


Figure 17: The frequency response for steer-torque-to-roll for all eight bicycles without the rider at 2 m/s.

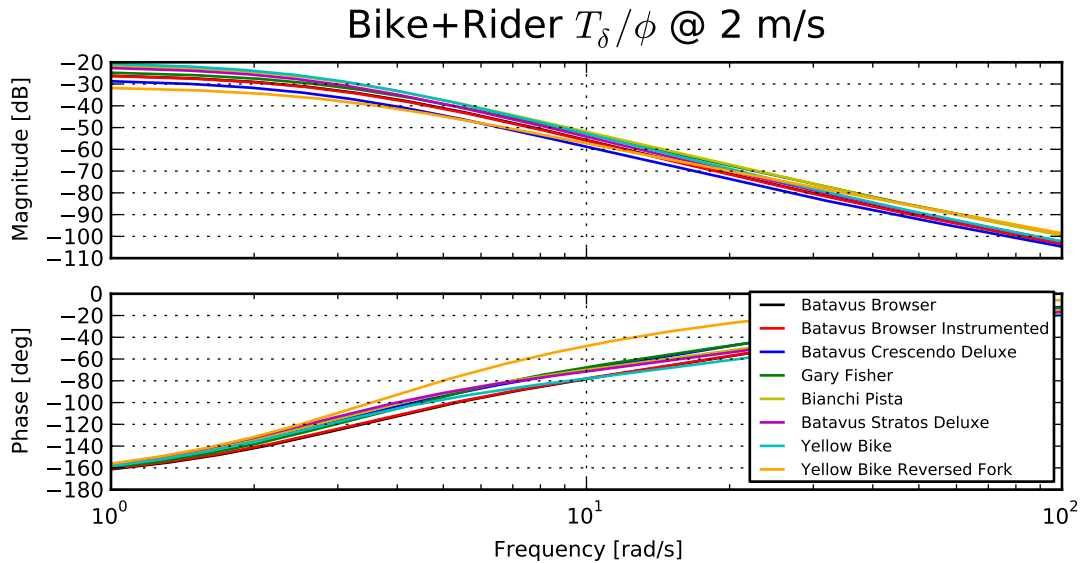


Figure 18: The frequency response for steer-torque-to-roll for all eight bicycles with the same rigid rider at 2 m/s.

- [7] MEIJAARD, J. P., PAPADOPOULOS, J. M., RUINA, A., AND SCHWAB, A. L. Linearized dynamics equations for the balance and steer of a bicycle: A benchmark and review. *Proceedings of the Royal Society A: Mathematical, Physical and Engineering Sciences* 463, 2084 (Aug 2007), 1955–1982.
- [8] MOORE, J. K., KOOIJMAN, J. D. G., HUBBARD, M., AND SCHWAB, A. L. A Method for Estimating Physical Properties of a Combined Bicycle and Rider. In *Proceedings of the ASME 2009 International Design Engineering Technical Conferences & Computers and Information in Engineering Conference, IDETC/CIE 2009* (San Diego, CA, USA, August–September 2009), ASME.
- [9] PATTERSON, W. B. *The Lords of the Chainring*. W. B. Patterson, 2004.
- [10] ROLAND JR., R. D., AND MASSING, D. E. A digital computer simulation of bicycle dynamics. Calspan Report YA-3063-K-1, Cornell Aeronautical Laboratory, Inc., Buffalo, NY, 14221, Jun 1971. Prepared for Schwinn Bicycle Company, Chicago, IL 60639.
- [11] SHARP, R. S. *Dynamical Analysis of Vehicle Systems*, vol. 497 of *CISM International Centre for Mechanical Sciences*. Springer Vienna, 2008, ch. Dynamics of Motorcycles: Stability and Control, pp. 183–230.
- [12] SINGH, D. V., AND GOEL, V. K. Stability of Rajdoot Scooter. Tech. rep., SAE, 1971. SAE Paper 710273.

A PARAMETER TABLES

The tabulated values for the both the physical parameters and the canonical matrix coefficients are shown in the following four tables. The uncertainties in the estimations of both the parameters and coefficients are also shown for the bicycle without a rider.

Table 2: The parameters for the eight bicycles with uncertainties in the estimations.

Parameter	B		B*		C		G		P		S		Y		Y*	
	Value	σ	Value	σ	Value	σ	Value	σ	Value	σ	Value	σ	Value	σ	Value	σ
w [m]	1.121	0.002	1.121	0.002	1.101	0.002	1.070	0.002	0.989	0.002	1.037	0.002	1.089	0.002	0.985	0.002
c [m]	0.069	0.002	0.068	0.002	0.083	0.002	0.072	0.002	0.062	0.002	0.056	0.002	0.047	0.002	0.180	0.002
λ [rad]	0.400	0.003	0.400	0.003	0.367	0.003	0.330	0.003	0.276	0.003	0.295	0.003	0.302	0.003	0.339	0.003
r_R [m]	0.3410	0.0001	0.3408	0.0001	0.3400	0.0001	0.3386	0.0001	0.3321	0.0001	0.3385	0.0001	0.3414	0.0001	0.3414	0.0001
m_R [kg]	3.11	0.02	3.11	0.02	3.96	0.02	1.94	0.02	1.38	0.02	3.96	0.02	2.57	0.02	2.57	0.02
I_{Rxx} [kg m ²]	0.0904	0.0004	0.0904	0.0004	0.0966	0.0004	0.0630	0.0003	0.0552	0.0002	0.0939	0.0004	0.0877	0.0004	0.0877	0.0004
I_{Ryy} [kg m ²]	0.152	0.001	0.152	0.001	0.144	0.001	0.101	0.001	0.076	0.001	0.154	0.001	0.149	0.001	0.149	0.001
x_B [m]	0.276	0.003	0.217	0.003	0.312	0.003	0.367	0.002	0.38	0.02	0.326	0.003	0.422	0.004	0.412	0.004
z_B [m]	-0.538	0.003	-0.622	0.003	-0.526	0.003	-0.499	0.003	-0.477	0.007	-0.483	0.003	-0.603	0.004	-0.618	0.004
m_B [kg]	9.86	0.02	14.71	0.02	9.18	0.02	4.48	0.02	4.49	0.02	7.22	0.02	3.31	0.02	3.31	0.02
I_{Bxx} [kg m ²]	0.527	0.002	0.866	0.005	0.500	0.002	0.283	0.001	0.290	0.002	0.373	0.002	0.2240	0.0009	0.2253	0.0009
I_{Bxz} [kg m ²]	-0.114	0.001	-0.181	0.004	-0.015	0.001	0.0559	0.0003	0.050	0.001	-0.0383	0.0004	0.0183	0.0001	0.0179	0.0001
I_{Byy} [kg m ²]	1.317	0.003	2.405	0.005	1.118	0.003	0.470	0.003	0.476	0.009	0.717	0.003	0.388	0.004	0.388	0.004
I_{Bzz} [kg m ²]	0.759	0.003	1.867	0.008	0.739	0.003	0.268	0.001	0.249	0.001	0.455	0.002	0.2164	0.0009	0.2150	0.0009
x_H [m]	0.867	0.004	0.867	0.004	0.907	0.005	0.960	0.006	0.906	0.005	0.911	0.004	0.948	0.004	0.919	0.005
z_H [m]	-0.748	0.003	-0.747	0.003	-0.803	0.003	-0.719	0.004	-0.732	0.002	-0.73	0.002	-0.788	0.002	-0.816	0.002
m_H [kg]	3.22	0.02	3.22	0.02	4.57	0.02	2.52	0.02	2.27	0.02	3.04	0.02	2.45	0.02	2.45	0.02
I_{Hxx} [kg m ²]	0.253	0.001	0.253	0.001	0.387	0.002	0.115	0.001	0.0980	0.0004	0.1768	0.0008	0.1452	0.0006	0.1475	0.0006
I_{Hxz} [kg m ²]	-0.072	0.0008	-0.072	0.0008	-0.076	0.001	-0.018	0.001	-0.0044	0.0003	-0.0273	0.0006	-0.0194	0.0005	-0.0172	0.0005
I_{Hyy} [kg m ²]	0.246	0.003	0.246	0.003	0.363	0.004	0.100	0.004	0.069	0.002	0.145	0.002	0.120	0.002	0.119	0.002
I_{Hzz} [kg m ²]	0.0956	0.0007	0.0956	0.0007	0.167	0.001	0.0227	0.0006	0.0396	0.0002	0.0446	0.0003	0.0292	0.0003	0.0294	0.0004
r_F [m]	0.3435	0.0001	0.3426	0.0001	0.3426	0.0001	0.3302	0.0001	0.3338	0.0001	0.3400	0.0001	0.3419	0.0001	0.3419	0.0001
m_F [kg]	2.02	0.02	2.02	0.02	3.55	0.02	1.50	0.02	1.58	0.02	3.33	0.02	1.90	0.02	1.90	0.02
I_{Fxx} [kg m ²]	0.0884	0.0004	0.0884	0.0004	0.0954	0.0004	0.0631	0.0003	0.0553	0.0002	0.0916	0.0004	0.0851	0.0003	0.0851	0.0003
I_{Fyy} [kg m ²]	0.149	0.001	0.149	0.001	0.166	0.001	0.106	0.001	0.106	0.001	0.157	0.001	0.147	0.002	0.147	0.002

Table 3: The canonical matrix coefficients for the eight bicycles with the uncertainty in the estimations.

Parameter	B		B*		C		G		P		S		Y		Y*	
	Value	σ														
M_{11}	6.21	0.03	9.39	0.06	7.44	0.04	3.33	0.02	3.07	0.03	4.88	0.02	3.79	0.02	3.96	0.02
M_{12}	0.33	0.01	0.36	0.01	0.69	0.02	0.37	0.01	0.33	0.01	0.41	0.01	0.33	0.01	0.68	0.01
M_{21}	0.33	0.01	0.36	0.01	0.69	0.02	0.37	0.01	0.33	0.01	0.41	0.01	0.33	0.01	0.68	0.01
M_{22}	0.220	0.002	0.223	0.002	0.373	0.006	0.152	0.005	0.155	0.003	0.203	0.003	0.165	0.003	0.301	0.006
C_{111}	0.0	NA														
C_{112}	4.39	0.03	4.97	0.04	6.45	0.04	3.44	0.02	3.44	0.04	4.85	0.03	3.63	0.02	4.70	0.03
C_{121}	-0.45	0.004	-0.451	0.004	-0.516	0.003	-0.344	0.004	-0.339	0.004	-0.489	0.003	-0.446	0.005	-0.554	0.005
C_{122}	0.58	0.01	0.63	0.01	1.11	0.03	0.57	0.02	0.55	0.01	0.75	0.02	0.52	0.01	1.05	0.02
K_{011}	-9.47	0.03	-13.31	0.05	-11.06	0.04	-5.2	0.03	-4.79	0.04	-8.18	0.03	-5.45	0.03	-5.57	0.03
K_{012}	-0.56	0.02	-0.59	0.02	-1.06	0.03	-0.57	0.02	-0.51	0.02	-0.71	0.02	-0.48	0.02	-0.94	0.02
K_{021}	-0.56	0.02	-0.59	0.02	-1.06	0.03	-0.57	0.02	-0.51	0.02	-0.71	0.02	-0.48	0.02	-0.94	0.02
K_{022}	-0.218	0.008	-0.228	0.008	-0.38	0.01	-0.185	0.007	-0.138	0.005	-0.206	0.007	-0.143	0.006	-0.311	0.008
K_{211}	0.0	NA														
K_{212}	8.50	0.03	11.67	0.05	10.14	0.04	5.15	0.03	5.19	0.04	8.39	0.03	5.54	0.03	6.16	0.03
K_{221}	0.0	NA														
K_{222}	0.60	0.02	0.62	0.02	1.05	0.03	0.60	0.02	0.58	0.02	0.78	0.02	0.53	0.01	1.03	0.02

Table 4: The parameters for the eight bicycles with the same rigid rider.

Parameter	B		B*		C		G		P		S		Y		Y*	
	Value	σ														
w [m]	1.121	NA	1.121	NA	1.101	NA	1.07	NA	0.989	NA	1.037	NA	1.089	NA	0.985	NA
c [m]	0.069	NA	0.068	NA	0.083	NA	0.072	NA	0.062	NA	0.056	NA	0.047	NA	0.18	NA
λ [rad]	0.4	NA	0.4	NA	0.367	NA	0.33	NA	0.276	NA	0.295	NA	0.302	NA	0.339	NA
r_R [m]	0.341	NA	0.341	NA	0.34	NA	0.339	NA	0.332	NA	0.338	NA	0.341	NA	0.341	NA
m_R [kg]	3.11	NA	3.11	NA	3.96	NA	1.94	NA	1.38	NA	3.96	NA	2.57	NA	2.57	NA
I_{Rxx} [kg m ²]	0.088	NA	0.088	NA	0.095	NA	0.063	NA	0.055	NA	0.092	NA	0.085	NA	0.085	NA
I_{Ryy} [kg m ²]	0.152	NA	0.152	NA	0.144	NA	0.101	NA	0.076	NA	0.154	NA	0.149	NA	0.149	NA
x_B [m]	0.289	NA	0.278	NA	0.293	NA	0.295	NA	0.296	NA	0.294	NA	0.297	NA	0.296	NA
z_B [m]	-1.04	NA	-1.027	NA	-1.043	NA	-1.073	NA	-1.072	NA	-1.052	NA	-1.087	NA	-1.088	NA
m_B [kg]	81.86	NA	86.71	NA	81.18	NA	76.48	NA	76.49	NA	79.22	NA	75.31	NA	75.31	NA
I_{Bxx} [kg m ²]	11.356	NA	11.759	NA	11.268	NA	9.851	NA	9.978	NA	10.947	NA	9.035	NA	8.988	NA
I_{Bxz} [kg m ²]	-1.968	NA	-1.67	NA	-2.043	NA	-2.067	NA	-2.123	NA	-2.111	NA	-2.12	NA	-2.098	NA
I_{Byy} [kg m ²]	12.218	NA	13.434	NA	11.96	NA	10.133	NA	10.271	NA	11.37	NA	9.324	NA	9.267	NA
I_{Bzz} [kg m ²]	3.124	NA	4.295	NA	3.105	NA	2.655	NA	2.648	NA	2.825	NA	2.633	NA	2.624	NA
x_H [m]	0.867	NA	0.867	NA	0.907	NA	0.96	NA	0.906	NA	0.911	NA	0.948	NA	0.919	NA
z_H [m]	-0.748	NA	-0.747	NA	-0.803	NA	-0.719	NA	-0.732	NA	-0.73	NA	-0.788	NA	-0.816	NA
m_H [kg]	3.22	NA	3.22	NA	4.57	NA	2.52	NA	2.27	NA	3.04	NA	2.45	NA	2.45	NA
I_{Hxx} [kg m ²]	0.253	NA	0.253	NA	0.387	NA	0.115	NA	0.098	NA	0.177	NA	0.145	NA	0.147	NA
I_{Hxz} [kg m ²]	-0.072	NA	-0.072	NA	-0.076	NA	-0.018	NA	-0.004	NA	-0.027	NA	-0.019	NA	-0.017	NA
I_{Hyy} [kg m ²]	0.246	NA	0.246	NA	0.363	NA	0.1	NA	0.069	NA	0.145	NA	0.12	NA	0.119	NA
I_{Hzz} [kg m ²]	0.096	NA	0.096	NA	0.167	NA	0.023	NA	0.04	NA	0.045	NA	0.029	NA	0.029	NA
r_F [m]	0.344	NA	0.343	NA	0.343	NA	0.33	NA	0.334	NA	0.34	NA	0.342	NA	0.342	NA
m_F [kg]	2.02	NA	2.02	NA	3.545	NA	1.5	NA	1.58	NA	3.334	NA	1.9	NA	1.9	NA
I_{Fxx} [kg m ²]	0.09	NA	0.09	NA	0.097	NA	0.063	NA	0.055	NA	0.094	NA	0.088	NA	0.088	NA
I_{Fyy} [kg m ²]	0.149	NA	0.149	NA	0.166	NA	0.106	NA	0.106	NA	0.157	NA	0.147	NA	0.147	NA

Table 5: The canonical matrix coefficients for the eight bicycles with the rigid rider.

Parameter	B		B*		C		G		P		S		Y		Y*	
	Value	σ														
M_{11}	102.78	NA	105.957	NA	104.002	NA	99.894	NA	99.631	NA	101.443	NA	100.353	NA	100.529	NA
M_{12}	1.536	NA	1.552	NA	2.195	NA	1.731	NA	1.608	NA	1.515	NA	1.216	NA	4.354	NA
M_{21}	1.536	NA	1.552	NA	2.195	NA	1.731	NA	1.608	NA	1.515	NA	1.216	NA	4.354	NA
M_{22}	0.249	NA	0.251	NA	0.417	NA	0.187	NA	0.185	NA	0.229	NA	0.182	NA	0.557	NA
C_{111}	0.0	NA														
C_{112}	26.395	NA	26.953	NA	30.154	NA	27.386	NA	28.964	NA	28.654	NA	25.623	NA	38.883	NA
C_{121}	-0.45	NA	-0.451	NA	-0.516	NA	-0.344	NA	-0.339	NA	-0.489	NA	-0.446	NA	-0.554	NA
C_{122}	1.037	NA	1.082	NA	1.722	NA	1.136	NA	1.118	NA	1.215	NA	0.868	NA	3.075	NA
K_{011}	-89.322	NA	-93.167	NA	-90.912	NA	-85.055	NA	-84.644	NA	-88.034	NA	-85.308	NA	-85.427	NA
K_{012}	-1.742	NA	-1.758	NA	-2.539	NA	-1.912	NA	-1.766	NA	-1.797	NA	-1.35	NA	-4.551	NA
K_{021}	-1.742	NA	-1.758	NA	-2.539	NA	-1.912	NA	-1.766	NA	-1.797	NA	-1.35	NA	-4.551	NA
K_{022}	-0.678	NA	-0.684	NA	-0.91	NA	-0.619	NA	-0.481	NA	-0.522	NA	-0.401	NA	-1.512	NA
K_{211}	0.0	NA														
K_{212}	74.125	NA	77.287	NA	77.857	NA	75.753	NA	82.885	NA	82.073	NA	75.55	NA	82.632	NA
K_{221}	0.0	NA														
K_{222}	1.57	NA	1.584	NA	2.3	NA	1.783	NA	1.802	NA	1.782	NA	1.295	NA	4.495	NA